



HAL
open science

Simulation Studies of Methane, Carbon Dioxide, Hydrogen, and Deuterium in ITQ-1 and NaX Zeolites

George K Papadopoulos, Doros N Theodorou

► **To cite this version:**

George K Papadopoulos, Doros N Theodorou. Simulation Studies of Methane, Carbon Dioxide, Hydrogen, and Deuterium in ITQ-1 and NaX Zeolites. *Molecular Simulation*, 2009, 35 (01-02), pp.79-89. 10.1080/08927020802468380 . hal-00515060

HAL Id: hal-00515060

<https://hal.science/hal-00515060>

Submitted on 4 Sep 2010

HAL is a multi-disciplinary open access archive for the deposit and dissemination of scientific research documents, whether they are published or not. The documents may come from teaching and research institutions in France or abroad, or from public or private research centers.

L'archive ouverte pluridisciplinaire **HAL**, est destinée au dépôt et à la diffusion de documents scientifiques de niveau recherche, publiés ou non, émanant des établissements d'enseignement et de recherche français ou étrangers, des laboratoires publics ou privés.

Simulation Studies of Methane, Carbon Dioxide, Hydrogen, and Deuterium in ITQ-1 and NaX Zeolites

Journal:	<i>Molecular Simulation/Journal of Experimental Nanoscience</i>
Manuscript ID:	GMOS-2008-0156.R1
Journal:	Molecular Simulation
Date Submitted by the Author:	06-Sep-2008
Complete List of Authors:	Papadopoulos, George; National Technical University of Athens, Chemical Engineering Theodorou, Doros; National Technical University of Athens, Chemical Engineering
Keywords:	Molecular dynamics, NaX, ITQ-1, Hydrogen, Carbon dioxide

SCHOLARONE™
Manuscripts

1
2
3 **SIMULATION STUDIES OF METHANE, CARBON DIOXIDE,**
4
5 **HYDROGEN, AND DEUTERIUM IN ITQ-1 AND NaX ZEOLITES**
6
7
8
9
10
11
12
13
14
15
16
17
18
19
20
21

22 George K. Papadopoulos and Doros N. Theodorou
23
24

25
26
27 *School of Chemical Engineering, National Technical University of Athens, 9 Heroon*
28
29 *Polytechniou Street, 157 80 Athens, Greece.*
30
31
32
33
34
35
36
37
38
39
40
41
42
43
44
45
46
47
48
49
50
51
52
53
54
55
56
57

58 **gkpap@chemeng.ntua.gr (George K. Papadopoulos)**
59

60 **doros@central.ntua.gr (Doros N. Theodorou)**

Abstract

The sorption dynamics of methane, carbon dioxide, hydrogen and deuterium in digitally reconstructed frameworks of ITQ-1 and NaX zeolites was investigated via atomistic and mesoscopic computer simulations. The loading dependence of the self-diffusivity proved to be affected by the energetic inhomogeneity of the sorption sites or/and their topology in the particular crystal. Collective (Maxwell – Stefan) and hence transport diffusivities are examined on the basis of sorbate–sorbate interactions via a jump diffusion model invoking Quasichemical mean field theory.

1. Introduction

The efficient design of nanoporous sorbents for reaction, separation, or environmental engineering processes requires a systematic study of the dynamical properties of sorbate molecules confined in the interior of these materials, which may be either crystalline, or amorphous. This type of study typically deals with a multicomponent sorbed phase inside a porous crystalline (e.g. zeolites) or amorphous (e.g. carbon molecular sieves, carbon nanotubes) sorbent material; under the conditions used in the majority of the applications, the solid phase can be considered static without seriously affecting the microscopic flow dynamics of the system [1].

Apart from the strong technology-oriented incentives for studying the dynamics of fluids in pore systems, revealing the physical aspects affecting the transport of the sorbed phase is of great fundamental interest. Among many classes of solids which serve as sorbent materials, structures exhibiting a high degree of order in their atomic-level structure, such as zeolites and more recently zeolitic shape-persistent analogues such as Zeolite Imidazolate, Metal- or Covalent-Organic Frameworks and Titanosilicates, have proved particularly promising. The significant advantage of these materials lies in their well-defined structural characteristics, namely the channel size and shape, the micropore connectivity and the charge distribution due, e.g., to the presence of more than one kinds of tetrahedral (T) atoms in their framework.

Following the macroscopic phenomenological approach, mass transport is studied in terms of flux vectors generated by density or chemical potential gradients in the sorbed phase by invoking either Fick's laws, or Maxwell-Stefan theory and the Onsager formulation, respectively [1 – 3]. The microscopic modelling of diffusion,

1
2
3 on the other hand, involves mostly deterministic Molecular Dynamics simulations in
4 equilibrium (MD) or non-equilibrium (NEMD) ensembles. Atomistic MD cannot
5 address time scales longer than microseconds with currently available computational
6 means. In order to overcome this problem, in cases where transport occurs as a
7 sequence of infrequent jumps between sites in the nanoporous medium, an alternative
8 way is to identify the sites where penetrant molecules spend most of their time,
9 compute intersite transition rates atomistically based on infrequent event theory, and
10 sample stochastic trajectories consisting of long sequences of jumps by Kinetic Monte
11 Carlo (KMC) simulation. KMC can clearly cover longer time scales; its use
12 presupposes a time scale separation between the time required for a molecule to
13 equilibrate within a state, and the waiting time before a jump to another state occurs.
14 Ref [1] and references therein describe in detail the methodology and the applicability
15 of dynamically corrected transition-state theory (TST) in conjunction with KMC to
16 diffusion studies of molecules sorbed in zeolites.

17
18
19
20
21
22
23
24
25
26
27
28
29
30
31
32
33
34
35
36
37
38
39 In this article we describe an attempt to relate the sorption and diffusion properties of
40 fluids such as hydrogen, methane, carbon dioxide and their mixtures in pure siliceous
41 and in anionic aluminosilicate zeolite frameworks containing interstitial and
42 exchangeable cations. We apply MD and proceed by utilizing the relationship of
43 transport coefficients and time correlation functions under the equilibrium *NVE*
44 ensemble, employing the Onsager regression hypothesis as it was later reformulated
45 in the context of Linear Response Theory [4]. The treatment of transport phenomena
46 via atomistic simulation has the advantage, in comparison with macroscopic
47 phenomenology, of predicting diffusivity magnitudes as well as their temperature,
48 loading and composition dependencies. Also, the predicted results are amenable to
49
50
51
52
53
54
55
56
57
58
59
60

1
2
3 comparison with mesoscopic and microscopic experimental measurements, such as
4 pulsed-field gradient NMR and quasi elastic neutron scattering, respectively, which
5
6
7
8 have been carried out on a variety of zeolite-guest systems [5 – 9].
9

10 11 12 13 14 15 **2. Computer modelling** 16

17 18 19 20 **2.1 Zeolite digitization** 21

22
23
24 The procedure we followed for reconstructing a digital crystal entails adopting the
25 unit cell geometric characteristics that correspond to the particular framework type
26 code; locating the position vectors of the “primary” framework atoms [10], from the
27 X-Ray-Diffraction pattern or neutron diffraction data of the crystal; and then applying
28 the symmetry operations of the space group to which the crystal belongs. The types
29 and position vectors of all framework and off-framework atoms of the unit cell, taking
30 into account their occupancy probability found from the XRD analysis or neutron
31 diffraction data, are finally generated to form a computer model of the unit cell.
32
33
34
35
36
37
38
39
40
41
42

43
44
45 We constructed a model for the ITQ-1 zeolite framework by employing a double unit
46 cell instead of the original hexagonal one, for convenience with periodic boundary
47 conditions. This new unit cell has an orthorhombic shape with axes
48 $a = 2 \sin(60^\circ) a'$; $b = a'$; $c = c'$ where a' and c' are the original hexagonal unit cell
49 axes. This procedure gave rise to a base-centered orthorhombic unit cell comprising
50 144 silicon and 288 oxygen atoms, with lattice points located at the centers of large
51 cavities of the zeolite [11].
52
53
54
55
56
57
58
59
60

1
2
3
4
5
6 The Si/Al ratio in the framework of the charged NaX ($\text{Na}_{86}\text{Al}_{86}\text{Si}_{106}\text{O}_{384}$) FAU crystal
7
8 not only determines the anionic charge per unit cell and thereby the number of
9
10 cations, but also affects the distribution of cations among the various kinds of sites
11
12 present in the unit cell. Because the Al and Si atoms are indistinguishable by the
13
14 XRD technique, in several positions the occupation probability for either type of T
15
16 atom is less than unity. The notation for the topology of these sites and their
17
18 occupancy by sodium cations have been reported in Ref. [10]. In this study we used
19
20 the model of Jaramillo and Auerbach [12], which explicitly distinguishes the Si and
21
22 Al atoms, attributing different partial charges to the oxygen framework atoms
23
24 according to their neighboring bonded T atoms. With this objective, we randomly
25
26 distributed Al atoms among the T sites of the framework up to the desired Si/Al ratio,
27
28 in such a way that Löwenstein's rule was fulfilled. In addition, the energy of the
29
30 crystal was minimized by means of a Simulated Annealing technique (Fig. 1).
31
32
33
34
35
36
37
38
39
40
41
42
43
44
45
46
47
48
49
50
51
52
53
54
55
56
57
58
59
60

< Fig. 1 >

45
46 The representation of the bed of NaX crystals discussed in section 3 was obtained
47
48 using a mesoscopic particle-based reconstruction method, where a prescribed porosity
49
50 and particle size are provided experimentally. The NaX final configuration was
51
52 arrived at through a successive series of energy minimizations by means of Molecular
53
54 Mechanics at constant particle number density. In this work, the zeolite bed consists
55
56 of octahedral NaX crystals, based on the experimentally measured bed density of 590
57
58 kg m^{-3} , the crystal density of 1530 kg m^{-3} and the porosity of 0.6; the mean crystal
59
60

size (edge length of the platonic octahedra) was equal to 30 μm [8].

2.2 Guest – host interactions

The triatomic linear molecule of carbon dioxide was modelled as two consecutive dumbbells sharing the central C atom, arranged on a straight line; partial charges were distributed around each molecule so as to reproduce experimental quadrupole moments [13]. The octapole moment of the methane molecule was ignored; thus, methane was represented as one neutral Lennard-Jones sphere with the parameters: $\varepsilon_{\text{CH}_4\text{-CH}_4}/k_B = 102.5 \text{ K}$, $\sigma_{\text{CH}_4\text{-CH}_4} = 0.362 \text{ nm}$; $\varepsilon_{\text{CH}_4\text{-O}}/k_B = 131.2 \text{ K}$, $\sigma_{\text{CH}_4\text{-O}} = 0.346 \text{ nm}$; $\varepsilon_{\text{CH}_4\text{-Na}}/k_B = 328.3 \text{ K}$, $\sigma_{\text{CH}_4\text{-Na}} = 0.294 \text{ nm}$. The above values resulted from performing a calibration with respect to measured sorption isotherms; they are able to reproduce satisfactorily a set of experimental data in a temperature range from 120 to 550 K found in Ref. [14]. Hydrogen was also modelled as a single Lennard-Jones site; its strength and size parameters resulted from calibration with respect to bulk experimental data, as explained in Refs 7 and 9 and the references therein.

For the short-ranged sorbate-sorbate and sorbate-zeolite atom interactions the Lennard-Jones potential was used, whereas for hydrogen, the approximation due to Feynman and Hibbs [15] was employed for all dispersion type interactions involved, in order to account for its quantum nature, i.e.,

$$U_q(r_{ij}) = U_{\text{LJ}}(r_{ij}) + \frac{\hbar^2}{24m_i k_B T} \left[\frac{\partial^2 U_{\text{LJ}}(r_{ij})}{\partial r_{ij}^2} + \frac{2}{r_{ij}} \frac{\partial U_{\text{LJ}}(r_{ij})}{\partial r_{ij}} \right], \quad (1)$$

1
2
3
4
5
6 where $U_{LJ}(r)$ is the Lennard-Jones potential function and m_r is the reduced mass of the
7
8 interacting pair of atoms, given by $m_r^{-1} = M_i^{-1} + M_j^{-1}$; M denotes molecular mass and
9
10 subscripts specify the pair interaction type, e.g. $H_2 - H_2$ ($i = j$), or H_2 with any atom in
11
12 the zeolite framework ($i \neq j$).
13
14

15
16
17
18 The long-ranged electrostatic interactions were handled by means of the Ewald
19
20 summation technique; the parameters used for the real and reciprocal part of the sums,
21
22 as well as the values of partial charges on the sorbate molecules and framework atoms
23
24 have been reported in detail elsewhere [10]. In order to reduce the computational
25
26 effort associated with both the short- and long-ranged sorbate-sorbent interactions,
27
28 when the sorbent was modelled as a rigid framework of atoms, as in the case of the
29
30 zeolite crystals studied in this work, we pretabulated these interactions prior to the
31
32 actual simulation run on a fine grid running through the pore space of the sorbent.
33
34 Sorbate-sorbate interactions, on the other hand, were computed explicitly at each step.
35
36
37
38
39
40

41
42 Sorption equilibria were studied by means of Grand Canonical Monte Carlo (GCMC)
43
44 simulations. These simulations also provided the starting configurations for our MD
45
46 simulations of transport. In the case of the faujasite NaX, we need to avoid stochastic
47
48 formation of the CO_2 and H_2 molecules inside sodalite cages during GCMC. Sodalite
49
50 cages are voluminous enough to accommodate one of these sorbate molecules; yet,
51
52 they are inaccessible to these molecules in reality, since the apertures connecting them
53
54 to the main pore space are too small to be traversed by the sorbates at any reasonable
55
56 rate. After the pretabulation of the entire potential, the interior of sodalite cages was
57
58 excluded from the sampling procedure during the Monte Carlo runs; thus, the
59
60

1
2
3
4 sampling of intracrystalline space was confined to the physically acceptable regions,
5
6 which are determined by the sizes of the CO₂ and H₂ molecules on the one hand and
7
8 openings of the sodalite framework on the other. Figure 2 shows our computation of
9
10 the electrostatic field within a certain plane in the NaX unit cell.
11
12

13
14
15 <Fig. 2>
16
17

18
19
20 The density, ρ , of sorbate molecules in the zeolite unit cells was computed by means
21
22 of GCMC sampling in the form of phase space averages under an imposed set of
23
24 chemical potential, μ , volume, V , and temperature, T , values. In particular, the
25
26 version of the GCMC algorithm due to Adams adopted here involves the quantity B ,
27
28 which is related to the excess chemical potential μ^{ex} of the sorbed phase through the
29
30 relation:
31
32

$$33 \quad B = \frac{1}{k_{\text{B}}T} \mu^{\text{ex}} + \ln \langle N \rangle, \quad (2)$$

34
35
36 while B is related to fugacity, f , of the bulk phase being in equilibrium with the sorbed
37
38 phase according to the equation
39
40
41
42

$$43 \quad Vf = k_{\text{B}}T \exp(B), \quad (3)$$

44
45
46 with k_{B} being the Boltzmann constant. In the remainder of this work, fugacity is
47
48 approximated by the pressure, assuming that the bulk phase behaves nearly as an ideal
49
50 gas.
51
52
53
54
55
56
57
58
59
60

2.3 Transport

The simulations of both methane and xenon were carried out in the standard MD *NVE* ensemble. The MD method creates a set of classical trajectories by integrating the equations of motion for a group of molecules within a fixed volume of zeolite. The equations of motion were formulated in Cartesian coordinates for all sorbate atoms. The sorbate molecules followed classical trajectories, whose time evolution was governed by Newton's equation of motion; the neglect of quantum effects is fully justified at the temperatures of interest here except for H₂, whose interactions are described by correcting the potentials as described above. The algorithms chosen for the solution of the differential equations of motion for all sorbates studied in this work belong to the category of Störmer-leapfrog integrators.

For the linear molecule of CO₂ the LEN algorithm [13, 16] was applied. It is a leapfrog algorithm in the sense that the quantities saved between time steps are the on-step orientation and the mid-step angular velocity. In particular, in place of angular velocity the rate of change of the bond vector, \mathbf{u} , is used. Synoptically, if $\hat{\mathbf{e}}$ is the unit bond vector fixed along the molecule axis, the torque \mathbf{T} on the molecule can be written as

$$\mathbf{T} = \sum_{\alpha} \mathbf{r}_{\alpha} \times \mathbf{f}_{\alpha} = \hat{\mathbf{e}} \times \sum_{\alpha} d_{\alpha} \mathbf{f}_{\alpha} = \hat{\mathbf{e}} \times \mathbf{g}, \quad (4)$$

with \mathbf{g} being the “turning force,” which can be determined from the nonbonded forces \mathbf{f}_α on each atom, the position vectors \mathbf{r}_α of each interaction site and the (algebraic) distances d_α of each atom α from the centre of mass of the linear molecule. In a linear molecule \mathbf{g} can be replaced by its component perpendicular to the molecular axis, \mathbf{g}_p , without affecting the torque. The component \mathbf{g}_p is defined as

$$\mathbf{g}_p = \mathbf{g} - (\hat{\mathbf{e}} \cdot \mathbf{g})\hat{\mathbf{e}}. \quad (5)$$

In order to avoid the use of angular velocity, the time derivative of the axis vector was used:

$$\mathbf{u} = \frac{d\hat{\mathbf{e}}}{dt}. \quad (6)$$

In this algorithm, we applied the constraint that the length of the $\hat{\mathbf{e}}$ vector remains unity by means of an undetermined Lagrange multiplier [16]. LEN showed remarkable stability, being capable of admitting very large time steps.

The elaboration of molecular dynamics results towards the estimation of transport coefficients, as mentioned in Section 1, relies on linear response theory, which provides the bridge between equilibrium time correlation functions and non-equilibrium response to weak perturbations. The theory also proves that the time integrals of autocorrelation functions are related to transport coefficients via relations known as Green-Kubo. In an averaged form which allows accumulating statistics over all the N molecules of the system possessing center-of-mass velocities, \mathbf{v}_a , where

$a = 1, \dots, N$, and for a three-dimensional system, these relations take the following forms for the self-diffusivity, D_s , and collective diffusivity, D_0 , respectively:

$$D_s = \frac{1}{3N} \int_0^\infty dt \left\langle \sum_{i=1}^N \mathbf{v}_i(t) \cdot \mathbf{v}_i(0) \right\rangle, \quad (7)$$

$$D_0 = \frac{1}{3N} \int_0^\infty dt \sum_{i=1}^N \sum_{j=1}^N \left\langle \mathbf{v}_i(t) \cdot \mathbf{v}_j(0) \right\rangle. \quad (8)$$

Alternatively, the above equations are usually used in their equivalent well-known Einstein form involving the position vectors of the particles, \mathbf{r}_i , i.e.,

$$D_s = \frac{1}{6N} \lim_{t \rightarrow \infty} \frac{d}{dt} \left\langle \sum_{i=1}^N [\mathbf{r}_i(0) - \mathbf{r}_i(t)]^2 \right\rangle, \quad (9)$$

$$D_0 = \frac{1}{6N} \lim_{t \rightarrow \infty} \frac{d}{dt} \left\langle \left[\sum_{i=1}^N [\mathbf{r}_i(0) - \mathbf{r}_i(t)] \right]^2 \right\rangle. \quad (10)$$

A general expression for the isothermal steady-state single component sorbate flow in the absence of external force fields can be written in Fickian form as follows

$$\mathbf{J} = -\mathbf{D}_t(\rho) \cdot \nabla \rho. \quad (11)$$

In the above equation, the vector \mathbf{J} is the overall macroscopic flux, expressed as the mean number of molecules flowing per unit cross-sectional area in a directional (anisotropic) medium due to a concentration (number density ρ) gradient, and \mathbf{D}_t is

1
2
3 the transport diffusivity tensor, which in general can be a function of concentration.
4
5 Therefore, in zeolite crystals or textured materials, transport, and consequently self-
6
7 and collective diffusivity, have a tensorial character (the reader is reminded that Eqs 7
8
9 – 10 are orientational averages); in other words the flux vector depends onto the
10
11 spatial orientation of the applied density gradient with respect to the crystal symmetry
12
13 axes. In an isotropic medium, Eq. 11 converts to the well known Fick's law defining
14
15 the scalar diffusivity.
16
17
18
19
20
21

22 The relation between the (orientationally averaged) transport and collective diffusivity
23
24 can be expressed through a Darken-type equation, i.e.,
25
26
27
28

$$D_1(\rho) = D_0(\rho) \frac{\partial \ln f}{\partial \ln \rho}. \quad (12)$$

29
30
31
32
33
34

35 In the preceding lines we have followed the Fickian phenomenological approach to
36
37 linking fluxes and concentration gradients. The interested reader can find an
38
39 analogous phenomenological development based on chemical potential gradients due
40
41 to Onsager, as well as the Stefan – Maxwell formulation, which is based on a balance
42
43 of forces exerted on the diffusing particles, in Refs [17, 18] and references therein.
44
45
46
47
48
49
50
51
52
53
54
55
56

57 3. Results and discussion

58
59
60

In this section we present results on sorption and diffusion computer experiments on selected siliceous and charged zeolite frameworks. Comparisons with experimental measurements are made, whenever possible.

<Fig. 3>

The sorbed phase concentration (loading) inside the crystal was computed by means of Grand Canonical Ensemble Monte Carlo. In Figure 3 the sorption isotherms of methane and carbon dioxide in ITQ-1 are shown for various sets of parameters used to describe the energetics of these systems in previous studies (see caption).

<Fig. 4>

The singlet density distribution $\rho^1(\mathbf{r}_1)$ for finding a molecule of methane at a certain position \mathbf{r}_1 , averaged over all occupancies and all configurations, $\mathbf{r} = \{\mathbf{r}_1, \mathbf{r}_2, \dots, \mathbf{r}_N\}$, inside the unit cell, given by the relation

$$\rho^1(\mathbf{r}_1) = \frac{1}{\Xi(\mu, V, T)} \sum_{N=1}^{\infty} \frac{\exp[\mu N / k_B T]}{(N-1)!} \int d^3 r_2 \dots d^3 r_N \exp[-U(\mathbf{r}) / k_B T] \quad (13)$$

is depicted in Figure 4; in this figure we selected low-value isodensity surfaces in order to depict the accessible (void) volume, indicating the two independent pore systems (Large Cavity, LC, and Sinusoidal Channel, SC) of this zeolite.

<Fig. 5>

1
2
3
4
5
6 In Figure 5, the experimentally measured sorption isotherms showing the results of
7
8 GCMC simulation for methane in faujasite X zeolite (Na_{86}X) are presented for two
9
10 temperatures; the location of sorbed methane molecules in the interior of supercages
11
12 in a snapshot from the simulation is depicted in Figure 6.
13
14

15
16
17
18 <Fig. 6>
19

20
21
22 Figure 7 presents the sorption isotherms of hydrogen and deuterium in Na_{86}X at 100
23
24 K. All the host-guest and guest-guest dispersive interactions have been described by
25
26 means of the Feynman-Hibbs potential mentioned in the previous section; the effect
27
28 of the quantum correction tends to reduce the well depth and shift the whole potential
29
30 function to the right, increasing the effective size of the sorbed molecules. In
31
32 particular, the lighter hydrogen molecule has a bigger effective size with weaker
33
34 energy interaction than deuterium. This relative difference is depicted in Figure 7,
35
36 where the deuterium is seen to be sorbed slightly more strongly than hydrogen.
37
38
39
40
41
42

43
44 <Fig. 7>
45
46
47

48
49 In Figure 8, self-diffusivity measurements of methane obtained from pulsed field
50
51 gradient NMR at 223 K [22] and 300 K [23] in faujasite X zeolite (Na_{86}X) are shown,
52
53 along with results of molecular dynamics under the same conditions.
54
55
56
57

58 <Fig. 8>
59
60

1
2
3 Predicted and measured values agree reasonably well, indicating a decrease of the
4 intra-crystalline CH₄ self-diffusivity as the concentration of sorbed phase increases
5
6 inside the NaX. The PFG - NMR and MD values appear significantly different at the
7
8 higher temperature, whereas the agreement at 223 K is more satisfactory. PFG -
9
10 NMR can sample also the inter-crystalline space in addition to the crystal interior,
11
12 which is solely sampled by molecular dynamics. The authors of Refs 22 and 23 state
13
14 that molecular exchange between the crystallites and the inter-crystalline space during
15
16 the observation time was negligible; hence, the measured signal can be solely
17
18
19
20
21
22
23
24

25 <Fig. 9>
26
27
28

29 attributed to the intra-crystalline motion. Therefore, the discrepancy at the higher
30
31 temperature may not be attributed to the different length scales probed by PFG - NMR
32
33 and MD. In previous studies [8, 24] it was shown that no matter what the intra-
34
35 crystalline diffusivity is, a major contribution to the measured effective diffusivity
36
37 must be expected from the inter-crystalline diffusivity, as well as from the fraction of
38
39 molecules in the intercrystalline space around the crystallites; both quantities are
40
41 highly temperature dependent.
42
43
44
45
46
47

48 In Figure 9, results from a Kinetic Monte Carlo simulation of inter-crystalline
49
50 diffusivity, of ethane in a bed of NaX crystals as a function of the (pressure and
51
52 temperature-dependent) mean free path in the gas phase are shown. The whole
53
54 procedure of our KMC involves collisions of molecules in the intercrystalline space
55
56 only, being treated in a mean field sense without explicitly considering colliding pairs.
57
58
59
60 The distance l traveled between successive collisions is picked from an exponential

1
2
3 distribution under the prevailing temperature T and pressure p , that is to say random
4 trajectories are generated in the void space of the medium in such a way that in the
5 bulk gas the lengths l between successive collisions follow the exponential
6 distribution expected from the Poisson stochastic sequence of intermolecular
7 collisions [8], that is to say, $\langle l \rangle f(l) = \exp(-l/\langle l \rangle)$; where $f(l)dl$ is the conditional
8 probability of having a collision-free trajectory length between l and $l + dl$, with the
9 mean value of l being denoted by $\langle l \rangle$. In the bulk gas phase, $\langle l \rangle$ is the molecular mean
10 free path $\lambda = k_B T / p \sigma_{\text{gas}}^2 \pi \sqrt{2}$, with σ_{gas} being the collision diameter of gas molecules.
11
12 Reflections upon collision with the isotropic crystal surface are assumed to be diffuse;
13 that is to say, a new direction of motion is generated according to the cosine law that
14 ensures equal flux of the emitted molecules from the surface through any elementary
15 area surrounding the collision point, irrespective of direction. In this way it is ensured
16 that the probability for a molecule to leave the surface per unit time per unit area on
17 the surface increases as the angle of reflection approaches the normal to the surface.
18
19
20
21
22
23
24
25
26
27
28
29
30
31
32
33
34
35
36
37
38
39
40

41 The left-hand side of Figures 9 shows the high-pressure regime ($\langle l \rangle = \lambda$) where the
42 overall diffusion process is controlled by frequent intermolecular collisions, and the
43 right-hand side of the same graph shows the behaviour in the low-pressure regime,
44 where molecular collisions with the surfaces of NaX crystals in the bed dominate the
45 overall diffusion process and mean free paths are long ($\langle l \rangle \gg \lambda$); obviously in the
46 latter regime, for λ values higher than $\langle l \rangle$ intercrystalline diffusivity remains unaltered
47
48
49
50
51
52
53
54
55
56
57 in the bed (see plateau in Figure 9).
58
59
60

<Fig. 10>

The results of Figure 10 for deuterium show a different trend from that observed with methane. Here, both quasi-elastic incoherent neutron scattering and molecular dynamics reveal an increase of the self-diffusivity of deuterium at low densities, followed by a plateau up to 8 molecules per supercage of NaX.

<Fig. 11>

<Fig. 12>

This behaviour may be explained on the basis of the different guest – host interactions for deuterium and methane (cf. Figures 11 and 12). These differences are reflected in the partial molar configurational internal energy of the sorbed species (i.e. devoid of the kinetic energy part, U_{ig}), $\bar{U}_s - U_{\text{ig}}$, as obtained from the covariance between number of molecules and potential energy, divided by the variance in the number of molecules in the course of a GCMC simulation, i.e.,

$$\bar{U}_s - U_{\text{ig}} = \frac{\langle NU \rangle - \langle N \rangle \langle U \rangle}{\langle N^2 \rangle - \langle N \rangle^2}. \quad (14)$$

In particular, it is seen that the total partial molar configurational internal energy increases abruptly in the case of deuterium and then decreases slightly as loading increases. Although in methane the net host–guest interactions exhibit a steady increase with loading, the total partial molar configurational internal energy of sorbed molecules remains almost constant; this is because the methane–methane part of the

1
2
3 partial molar configurational energy decreases much faster with occupancy compared
4 to the sorbed deuterium-deuterium interactions (cf. insets in Figures 11 and 12). As a
5 consequence, deuterium perceives a higher energetic heterogeneity within NaX than
6 does methane. The most attractive host sites (i.e., those presenting the deepest
7 minima in the host-hydrogen potential energy field) are occupied first, the molecules
8 residing in them being less mobile; additional molecules at higher occupancy are
9 more loosely bound. Thus, an increase in deuterium loading is accompanied by an
10 increase in self-diffusivity (Figure 10). On the other hand, methane, which feels a
11 practically homogeneous energetic environment, exhibits a decrease of self-diffusivity
12 with loading because of enhanced intermolecular collisions at high loadings (Figure
13 8). The above observed difference in host-guest interactions for the two molecules
14 gives rise to opposite trends in the concentration dependence of self-diffusivities.
15
16
17
18
19
20
21
22
23
24
25
26
27
28
29
30
31
32
33

34 <Fig. 13>
35
36
37
38

39 In a simulation study on ITQ-1 we found a shallow maximum with occupancy in the
40 self-diffusivity of methane. In this zeolite the pore structure is more complicated than
41 the one of NaX, with two disconnected pore systems. Two-dimensional diffusion can
42 occur in each pore system with the D_{zz} element of the diffusivity tensor being zero.
43 One pore system exhibits large cavities communicating through narrow necks (Figure
44 4). In this type of structure we found that the concentration dependence of the self-
45 diffusivity can be strongly affected by the sorbate density distribution along the
46 narrow interconnections [25]. Figure 13 shows such a sequence of computed
47 probability densities for CO_2 and CH_4 for various total concentrations inside the ITQ-
48 1 crystal. Methane prefers to reside at the top and bottom of the large cavities. As
49
50
51
52
53
54
55
56
57
58
59
60

1
2
3 occupancy increases, it tends to occupy the middle regions of the large cavities more;
4
5 this facilitates entry into and passage through the narrow necks emanating from the
6
7 middle regions of the large cavities (see Figure 4), leading to the observed shallow
8
9 maximum in self-diffusivity [25].
10
11

12
13
14
15 <Fig. 14>
16

17
18
19 In Figures 14 the collective (or else the Maxwell – Stefan [17]) diffusivity and the
20
21 transport diffusivity of methane and carbon dioxide in ITQ-1 are presented. The
22
23 observed behaviour for carbon dioxide is a continuous decrease of collective
24
25 diffusivity as the fugacity (pressure of bulk phase) of the sorbed phase increases. On
26
27 the other hand, methane exhibits a slight maximum.
28
29
30
31
32
33

34 <Fig. 15>
35
36
37

38
39 The effect of concentration on the collective diffusivity of hydrogen in NaX is
40
41 presented in Figure 15; in this graph, contrary to the trend observed for methane in the
42
43 same zeolite, collective diffusivity shows initially an increase up to a slight maximum
44
45 just beyond 4 molecules per supercage. In order to interpret this behaviour we have
46
47 previously invoked the Reed and Ehrlich theory, [26] according to which the
48
49 occupancy dependence of the collective (or corrected, or else Maxwell – Stefan)
50
51 diffusivity can be related to the strength of interactions between the sorbate
52
53 molecules. In the lattice model considered by Reed and Ehrlich, this strength is
54
55 quantified through the nearest neighbor interaction energy parameter, w , introduced in
56
57 conjunction with the Quasichemical mean field theory of sorption; the coordination
58
59
60

1
2
3
4 number, z , of the lattice and the saturation capacity ρ_m are additional parameters of
5
6 the model [5, 26].
7
8
9

10
11 **<Fig. 16>**
12
13

14
15 Figure 16 gives an indicative example of the use of Reed - Ehrlich theory for the case
16 of hydrogen in NaX. The parameters w , z , were estimated by means of fitting to the
17 simulation data; ρ_m was computed by GCMC. According to this simple theory, the
18 presence of a maximum in the collective diffusivity is a consequence of a weak
19 (considerably less than $k_B T$) dispersion interaction between co-sorbed hydrogen
20 molecules. In the same graph is shown the predicted collective diffusivity of
21 deuterium; this is described better by the theoretical Reed and Ehrlich curve. The
22 differences seen between H₂ and D₂ in Figure 16 correspond to more attractive
23 sorbate – sorbate interactions between D₂ molecules as compared to H₂ molecules.
24
25
26
27
28
29
30
31
32
33
34
35
36
37
38
39

40
41 **<Fig. 17>**
42
43

44 Figure 17 shows three other theoretical plots based on the Reed and Ehrlich theory,
45 constructed for more attractive sorbate-sorbate interactions. These exhibit
46 completely different loading dependences, which are reminiscent of the behaviours of
47 methane and carbon dioxide in ITQ-1 (see Figure 14). One should note that the
48 model of jumps in a lattice considered by Reed and Ehrlich theory is very simplified,
49 providing only a qualitative explanation of the occupancy dependence of the
50 collective diffusivity of fluids under confinement.
51
52
53
54
55
56
57
58
59
60

4. Conclusions

We have performed simulations at atomistic and mesoscopic levels in order to explore the concentration dependence of the sorbed phase dynamics of polar and non-polar fluids in digitally reconstructed purely siliceous as well as counterion-containing aluminosilicate zeolite frameworks.

For the former category we selected a typical representative belonging to Framework Type Code MWW, the ITQ-1. Sorption and diffusion in this zeolite should differ only slightly from those in the protonated version of its aluminum-containing analogue, MCM-22. In the latter class, a representative of the FAU framework type, Na₈₆X, was reconstructed. The Si/Al ratio in the frame of this type determines the anionic charge, and therefore the number of cations (counterions) per unit cell. It also affects the distribution of counterions among the various kinds of site present in the unit cell. In the modeling distinct coulombic charges were attributed to all atoms in the framework.

Our molecular dynamics results for the self-diffusivity of methane in NaX show that D_s decreases as the loading increases; this is in agreement with earlier PFG – NMR intra-crystalline self-diffusivity measurements of other groups [22, 23]. Furthermore, our Kinetic Monte Carlo mesoscopic simulations of inter-crystalline diffusion in an assemblage of NaX crystals predict that the inter-crystalline diffusivity, not captured by atomistic MD simulations, becomes important at high temperatures where Knudsen diffusion becomes dominant.

1
2
3
4
5
6 The self-diffusivity of deuterium in NaX, which is predicted in good agreement with
7
8 recent QENS measurements, exhibits a monotonic increase with loading. The
9
10 energetic heterogeneity experienced by deuterium molecules in NaX proves to be
11
12 responsible for this peculiar behaviour, also observed in the case of hydrogen in NaX.
13
14 Within ITQ-1, which possesses large elongated cavities with strongly attractive
15
16 regions at their top and bottom, connected along their waists by narrow, strongly
17
18 attractive pores, the self-diffusivity of methane exhibits a shallow maximum. A
19
20 mesoscopic Diffusion through Spatial Discretization approach recently developed in
21
22 our group [25] is able to explain this trend.
23
24
25
26
27
28

29 Collective (Maxwell – Stefan) and transport diffusivities of carbon dioxide and
30
31 methane in ITQ-1 and also of hydrogen and deuterium in NaX were studied via
32
33 atomistic molecular dynamics simulations. Their concentration dependence was
34
35 investigated on the basis of the sorbate – sorbate interaction strength invoked by
36
37 Quasichemical mean field theory in conjunction with the simple model of Reed and
38
39 Ehrlich.
40
41
42
43
44
45

46 **Acknowledgments**

47
48 We are grateful to Dr E. Pantatosaki and Mr M. Sant for their contribution in the
49
50 computational work. Support by the European Union via the FP6-Marie Curie
51
52 Research Training Network “INDENS” (MRTN-CT-2004-005503) is gratefully
53
54 acknowledged.
55
56
57
58
59
60

References

- [1] D. N. Theodorou, R. Q. Snurr, A. T. Bell, *Molecular dynamics and diffusion in microporous materials*, in *Comprehensive Supramolecular Chemistry*, Vol. 7, G. Alberti and T. Bein (Eds.), Elsevier, Oxford, 1996, p. 507.
- [2] Auerbach, S. M.F. Jousse, D. P. Vercauteren, *Dynamics of sorbed molecules in zeolites*, in *Computer Modelling of Microporous and Mesoporous Materials*, C. R. A. Catlow, R. A. van Santen, B. Smit (Eds.), Elsevier, Amsterdam, 2004, p. 49.
- [3] G. K. Papadopoulos and D. N. Theodorou, *Computer simulation of sorption and transport in zeolites*, in *Handbook of Heterogeneous Catalysis*, 2nd Ed., Vol. 3, G. Ertl, H. Knözinger, F. Schüth and J. Weitkamp (Eds.), p. 1662, Wiley - VCH, Weinheim (2008).
- [4] J. P. Hansen, I. R. McDonald, *Theory of simple liquids*, Academic Press, London, 1986.
- [5] G. K. Papadopoulos, H. Jobic, and D. N. Theodorou, *Transport diffusivity of N₂ and CO₂ in silicalite: Coherent quasielastic neutron scattering measurements and molecular dynamics simulations*, *J. Phys. Chem. B*, **108** (2004), p. 12748.
- [6] G. K. Papadopoulos, *Diffusivity of CH₄ in model silica nanopores: Molecular dynamics and quasichemical mean field theory*, *Mol. Simul.*, **31** (2005), p. 57.

1
2
3 [7] A. Kumar, H. Jobic and S. K. Bhatia, *Quantum Effects on Adsorption and*
4
5
6 *Diffusion of Hydrogen and Deuterium in Microporous Materials*, J. Phys. Chem B,
7
8 **110** (2006), p. 16666.
9

10
11
12
13
14
15 [8] G. K. Papadopoulos, D. N. Theodorou, S. Vasenkov and J. Kärger, *Mesoscopic*
16
17 *simulations of the diffusivity of ethane in beds of NaX zeolite crystals: Comparison*
18
19 *with pulsed field gradient NMR measurements*, J. Chem. Phys., **126** (2007), p.
20
21 094702.
22
23

24
25
26
27
28
29 [9] E. Pantatosaki, G. K. Papadopoulos, H. Jobic, and D. N. Theodorou, *A combined*
30
31 *atomistic simulation and quasielastic neutron scattering study of the low-temperature*
32
33 *dynamics of hydrogen and deuterium confined in NaX zeolite*, J. Phys. Chem. B
34
35 (2008), in press.
36
37

38
39
40
41 [10] E. Pantatosaki and G. K. Papadopoulos, *On the computation of long-range*
42
43 *interactions in fluids under confinement: Application to pore systems with various*
44
45 *types of spatial periodicity*, J. Chem. Phys., **127** (2007), p. 164723.
46
47
48

49
50
51 [11] J.-M. Leyssale, G. K. Papadopoulos and D. N. Theodorou, *Sorption*
52
53 *thermodynamics of CO₂, CH₄ and their mixtures in the ITQ-1 zeolite as revealed by*
54
55 *molecular simulations*, J. Phys. Chem. B, **110** (2006), p. 22742.
56
57

58
59
60 [12] D. E. Jaramillo and S. M. Auerbach, *New force field for Na cations in faujasite-*

1
2
3
4
5
6
7
8
9
10
11
12
13
14
15
16
17
18
19
20
21
22
23
24
25
26
27
28
29
30
31
32
33
34
35
36
37
38
39
40
41
42
43
44
45
46
47
48
49
50
51
52
53
54
55
56
57
58
59
60

type zeolites, J. Phys. Chem. B **103** (1999), p. 9589.

[13] K. Makrodimitris, G. K. Papadopoulos and D. N. Theodorou, Prediction of *permeation properties of CO₂ and N₂ through silicalite via molecular simulations*, J. Phys. Chem. B, **105** (2001), p. 777, and references therein.

[14] E. V. Chkhaidze, A. A. Fomkin, V.V. Sepinskii, G. V. Tsitsishvili, *Adsorption of methane on NaX zeolite in the subcritical and supercritical regions*, Bull. Acad. Sci. USSR, Div. Chem. Sci., **34** (1985), p. 886.

[15] R. P. Feynman and A. R. Hibbs, *Quantum Mechanics and Path Integrals*, McGraw-Hill, New York, 1965

[16] D. Fincham, *Leapfrog Rotational Algorithms for Linear Molecules*, Mol. Simul. **11** (1993), p. 79.

[17] D. Dubbeldam and R. Q. Snurr, *Recent developments in the molecular modeling of diffusion in nanoporous materials*, Mol. Simul., **33** (2007), p. 305.

[18] R. Krishna and J. M. van Baten, *Onsager coefficients for binary mixture diffusion in nanopores*, Chem. Eng. Sci. (2008), in press.

[19] S. J Goodbody, K.Watanabe, D. MacGovan, J. Walton, and N. Quirke, *Molecular simulation of methane and butane in silicalite*, J. Chem. Soc. Faraday Trans., **87** (1991), p. 1951.

- 1
2
3
4
5
6 [20] D. Dubbeldam, S. Calero, T. J. H. Vlugt, R. Krishna, T. Maesen, and B. Smit,
7
8 *United atom force field for alkanes in nanoporous materials*, J. Phys. Chem. B, **108**
9
10 (2004), p. 12301.
11
12
13
14
15 [21] J. G. Harris, K. H. Yung, *Carbon dioxide's liquid-vapor coexistence curve and*
16
17 *critical properties as predicted by a simple molecular model*, J. Phys. Chem., **99**
18
19 (1995), p. 12021.
20
21
22
23
24
25
26 [22] J. Kärger, H. Pfeifer, M. Rauscher, and A. Walter, *Self-diffusion of n-paraffins in*
27
28 *NaX zeolite*, J. C. S. Faraday I, **76** (1980), p. 717.
29
30
31
32
33
34 [23] J. Caro, M. Bülow, and W. Schirmer, *Microdynamics of methane, ethane and*
35
36 *propane in ZSM-5 type zeolites*, J. Chem. Soc., Faraday Trans. I, **81** (1985), p. 2541.
37
38
39
40
41 [24] O. Geier, S. Vasenkov, E. Lehmann, J. Kärger, U. Schemmert, R. Rakoczy, J.
42
43 *Weitkamp, Interference microscopy investigation of the influence of regular*
44
45 *intergrowth effects in MFI-type zeolites on molecular uptake*, J. Phys. Chem. B, **105**
46
47 (2001), p. 10217.
48
49
50
51
52
53 [25] M. Sant, G. K. Papadopoulos and D. N. Theodorou, *A second-order Markov*
54
55 *process for modeling diffusive motion through spatial discretization*, J. Chem. Phys.
56
57 **128** (2008), p. 024504; M. Sant, J.-M. Leyssale, G. K. Papadopoulos, and D.N.
58
59 Theodorou, in preparation.
60

- 1
2
3
4
5 [26] D. A. Reed and G. Ehrlich, *Surface diffusion, atomic jump rates and*
6 *thermodynamics*, Surface Sci. **102** (1981), p. 588.
7
8
9
10
11
12
13
14
15
16
17
18
19
20
21
22
23
24
25
26
27
28
29
30
31
32
33
34
35
36
37
38
39
40
41
42
43
44
45
46
47
48
49
50
51
52
53
54
55
56
57
58
59
60

For Peer Review Only

Captions to figures

Figure 1. Indicative total energy plateau during the simulated annealing minimization procedure in NaY [10]; the last runs locating the minimum global energy of the crystal are depicted in the inset.

Figure 2. Indicative computed electrostatic field contours for NaX, at $z = 2.27$ nm. The sodalite interiors, which are removed from the mapping, are evident as open circular regions.

Figure 3. Sorption isotherms of CH₄ for two sets of parameters [19, 20] and of the EPM2 model of CO₂ [21] at various temperatures within ITQ-1.

Figure 4. Lowest value isodensity surface of CH₄ in ITQ-1 at a total loading of 20.4 (LC) plus 8.6 (SC) molecules per unit cell

Figure 5. Measured [14] and predicted sorption isotherms of CH₄ in NaX.

Figure 6. Distribution of CH₄ (white spheres) in the Na₈₆X framework, depicting the host sorption areas (supercages) at a loading of 9.16 molecules per supercage at 300 K.

Figure 7. Simulated sorption isotherms at 100 K for D₂ (red symbols) and H₂ (green symbols) in NaX.

1
2
3 **Figure 8.** Comparison of self-diffusivity data obtained via PFG-NMR measurements
4 at 223 K [22] and 300 K [23], with molecular dynamics simulations for CH₄ in NaX
5 as a function of loading.
6
7
8
9

10
11
12 **Figure 9.** Intercrystalline self-diffusivity of C₂H₆ computed via Kinetic Monte Carlo
13 simulation in a reconstructed bed of octahedral NaX crystals with porosity 0.40 as a
14 function of mean free path λ .
15
16
17
18
19

20
21
22 **Figure 10.** Self-diffusivities of D₂ in NaX measured by QENS at 100 K [9] (open
23 symbols), and results computed by MD under the same conditions (filled symbols) as
24 a function of sorbate loading.
25
26
27
28
29

30
31
32 **Figure 11.** Partial molar configurational internal energy, of sorbed H₂ in NaX
33 calculated from GCMC simulations at a temperature of 100 K and various loadings
34 (squares); contributions to this quantity from H₂ – NaX interactions (triangles), and
35 from H₂ – H₂ interactions (inset) are also shown.
36
37
38
39
40
41

42
43
44 **Figure 12.** Same as Figure 11 for CH₄ in NaX at 300 K.
45
46
47

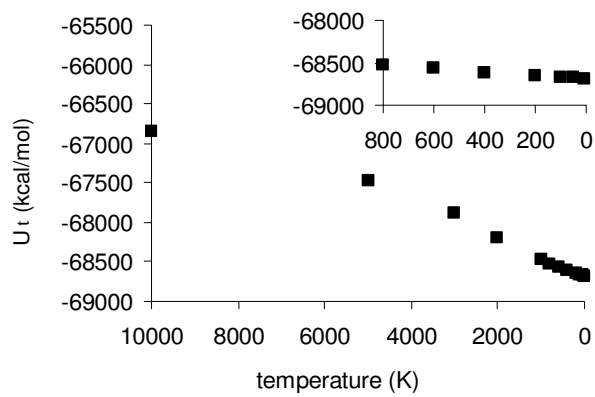
48
49 **Figure 13.** xy probability densities for CO₂ (a, b, c) and CH₄ (d, e, f) sorbates in the
50 LC pore system of ITQ-1 at $T = 250$ K. The pressure is 0.006 atm (a, d), 0.95 atm (b,
51 e) and 52 atm (c, f).
52
53
54
55
56

57
58 **Figure 14.** Collective and transport diffusivities at 300 K for CH₄ (top) and CO₂
59 (bottom) in ITQ-1 as a function of pressure of the bulk phase at equilibrium.
60

1
2
3
4
5
6 **Figure 15.** Collective (triangles) and transport (circles) diffusion coefficients
7
8 predicted via MD as a function of H₂ loading in NaX.
9

10
11
12 **Figure 16.** Normalized simulated and experimental collective diffusivities for
13 hydrogen (circles) and deuterium (triangles) in NaX versus fractional occupancies $\theta =$
14 ρ / ρ_m , where ρ_m is the saturation capacity of NaX for H₂; lines correspond to
15 theoretical predictions from the Reed and Ehrlich model [26].
16
17
18
19
20
21
22
23
24

25 **Figure 17.** Normalized collective diffusivities versus fractional occupancies θ for
26 various w values corresponding to theoretical predictions from the Reed and Ehrlich
27 model [26].
28
29
30
31
32
33
34
35
36
37
38
39
40
41
42
43
44
45
46
47
48
49
50
51
52
53
54
55
56
57
58
59
60

**Fig. 1**

1
2
3
4
5
6
7
8
9
10
11
12
13
14
15
16
17
18
19
20
21
22
23
24
25
26
27
28
29
30
31
32
33
34
35
36
37
38
39
40
41
42
43
44
45
46
47
48
49
50
51
52
53
54
55
56
57
58
59
60

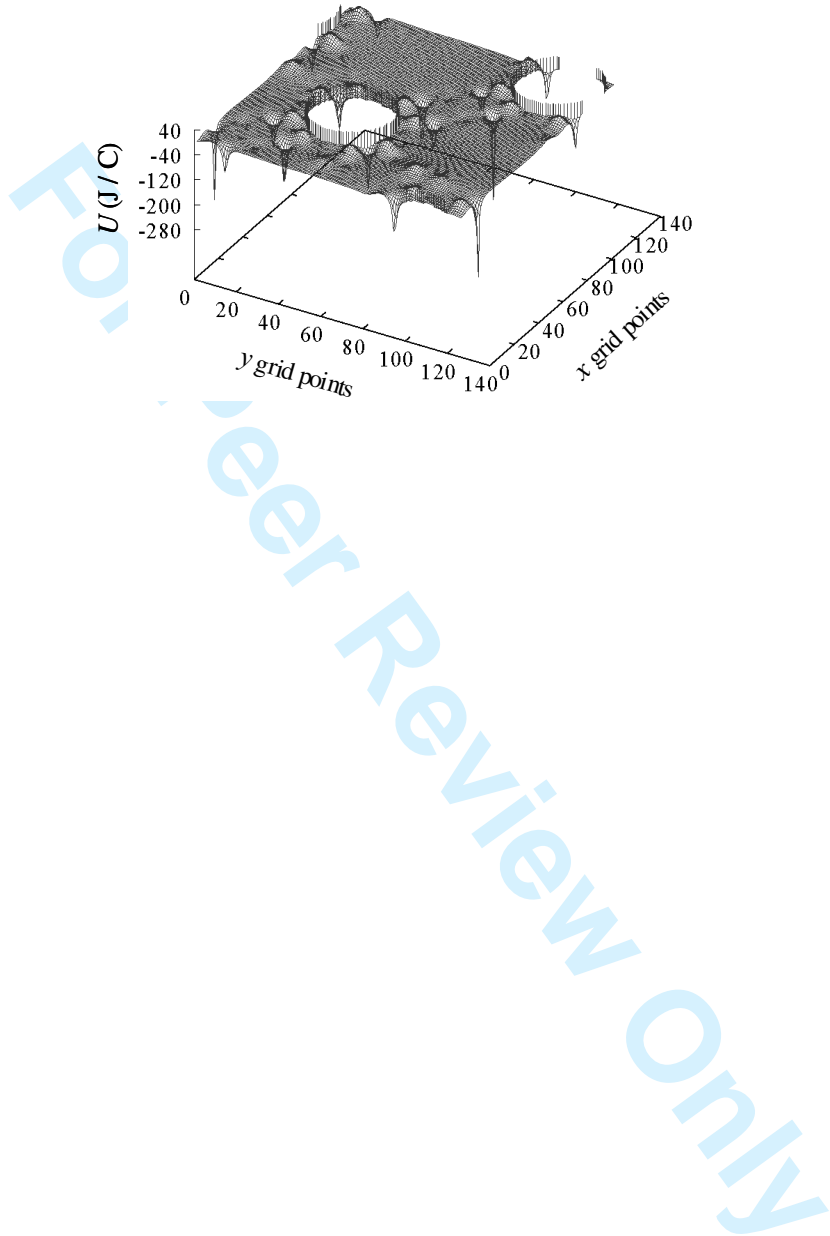


Fig. 2

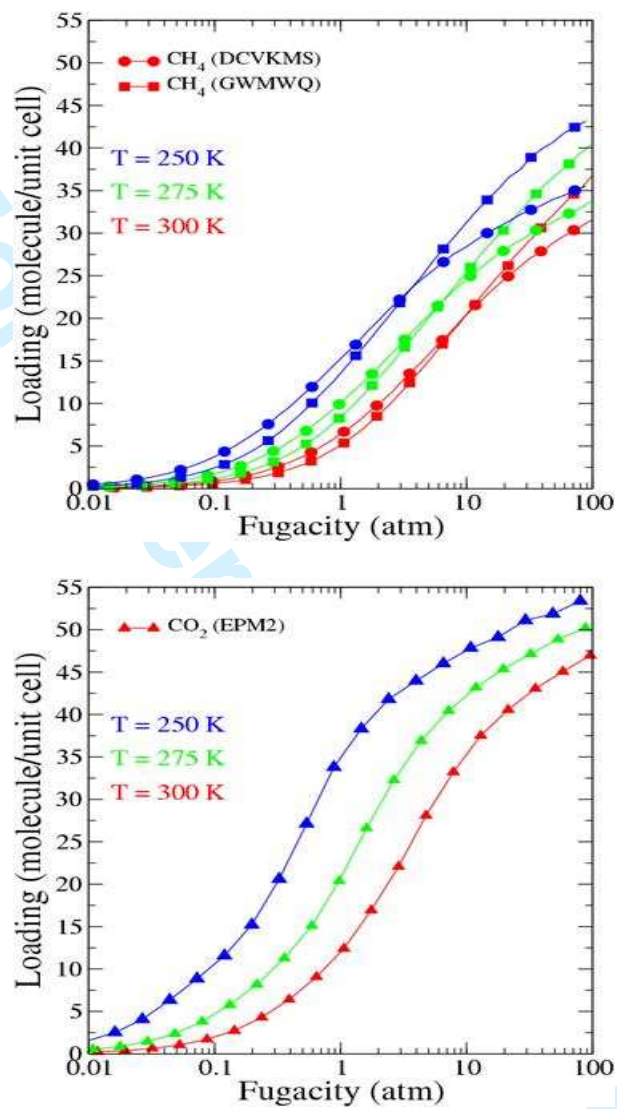


Fig. 3

1
2
3
4
5
6
7
8
9
10
11
12
13
14
15
16
17
18
19
20
21
22
23
24
25
26
27
28
29
30
31
32
33
34
35
36
37
38
39
40
41
42
43
44
45
46
47
48
49
50
51
52
53
54
55
56
57
58
59
60

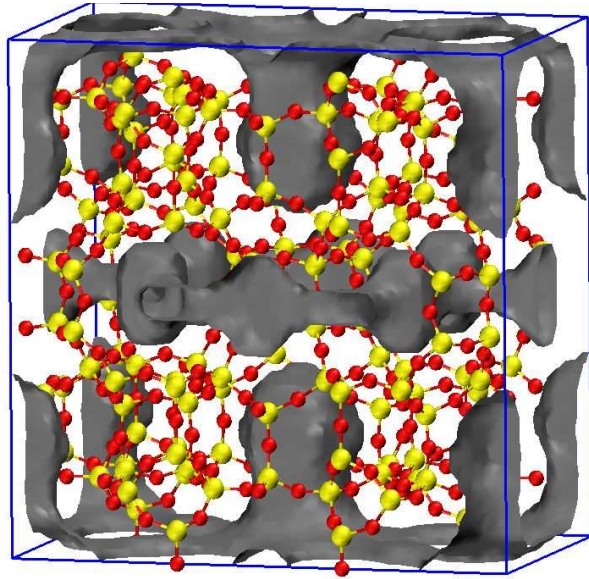


Fig. 4

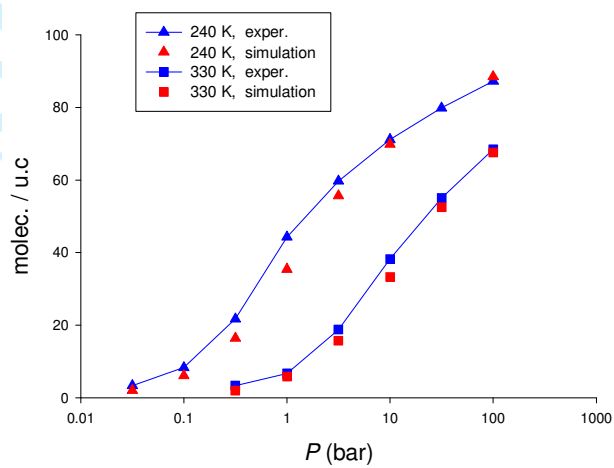


Fig. 5

1
2
3
4
5
6
7
8
9
10
11
12
13
14
15
16
17
18
19
20
21
22
23
24
25
26
27
28
29
30
31
32
33
34
35
36
37
38
39
40
41
42
43
44
45
46
47
48
49
50
51
52
53
54
55
56
57
58
59
60

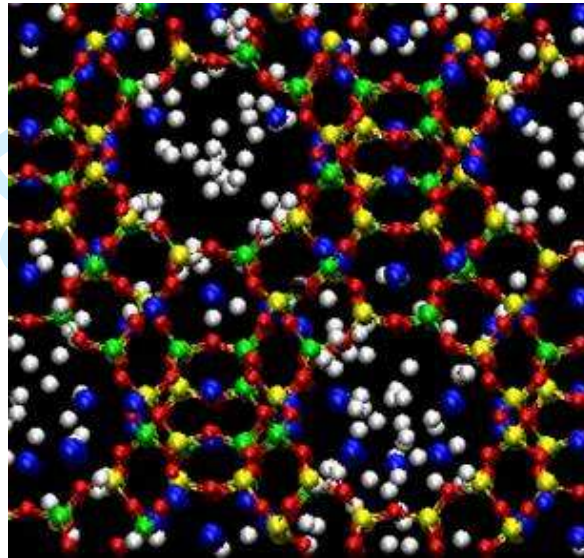


Fig. 6

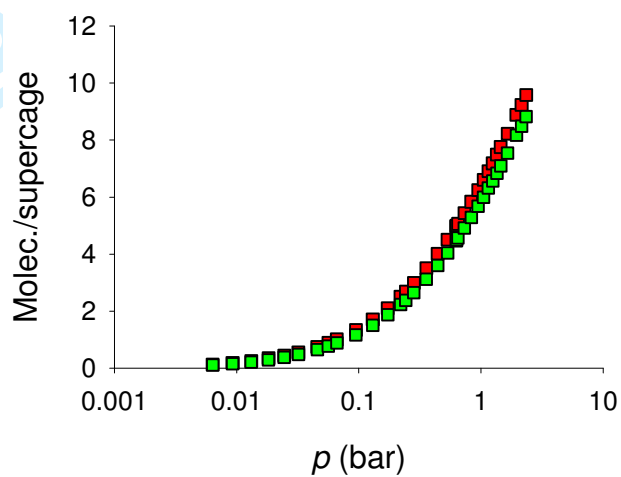


Fig. 7

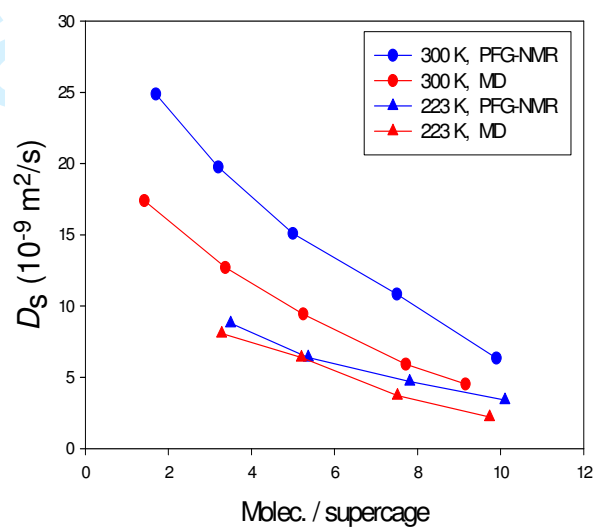
1
2
3
4
5
6
7
8
9
10
11
12
13
14
15
16
17
18
19
20
21
22
23
24
25
26
27
28
29
30
31
32
33
34
35
36
37
38
39
40
41
42
43
44
45
46
47
48
49
50
51
52
53
54
55
56
57
58
59
60

Fig. 8

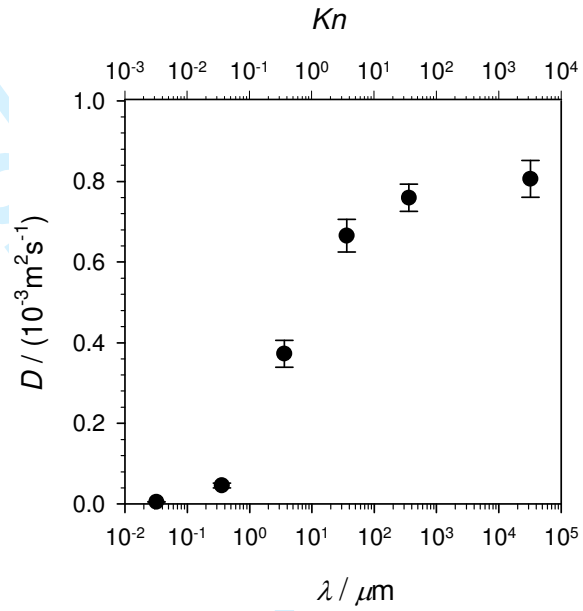


Fig. 9

1
2
3
4
5
6
7
8
9
10
11
12
13
14
15
16
17
18
19
20
21
22
23
24
25
26
27
28
29
30
31
32
33
34
35
36
37
38
39
40
41
42
43
44
45
46
47
48
49
50
51
52
53
54
55
56
57
58
59
60

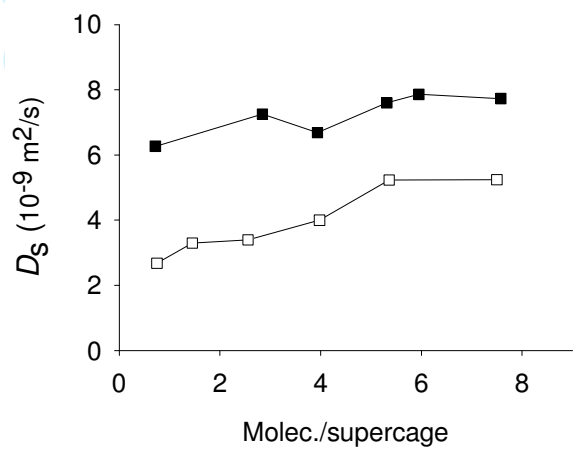


Fig. 10

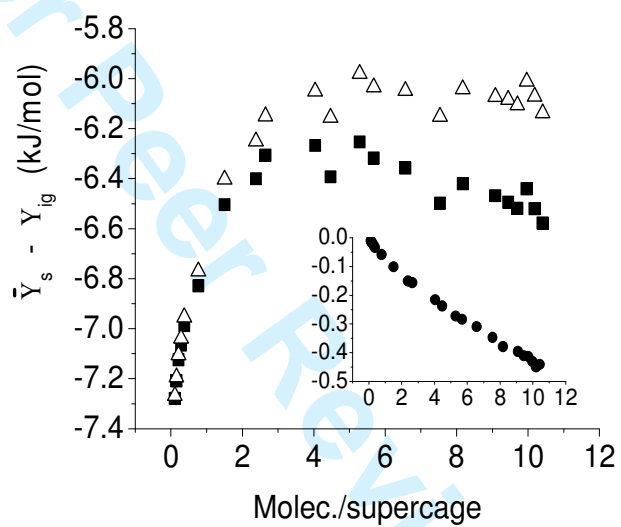


Fig. 11

1
2
3
4
5
6
7
8
9
10
11
12
13
14
15
16
17
18
19
20
21
22
23
24
25
26
27
28
29
30
31
32
33
34
35
36
37
38
39
40
41
42
43
44
45
46
47
48
49
50
51
52
53
54
55
56
57
58
59
60

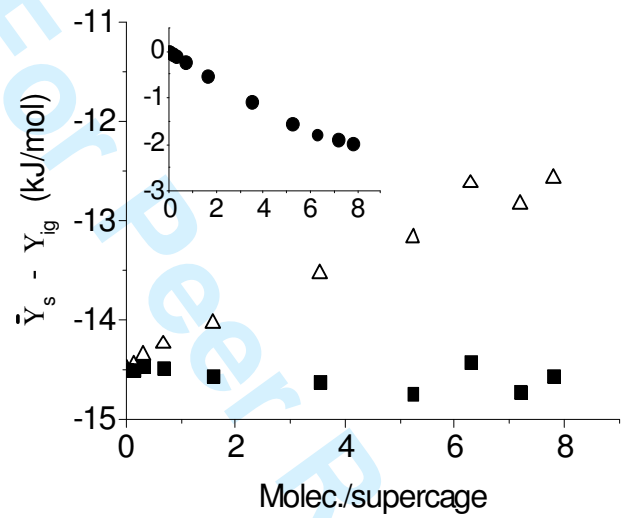


Fig. 12

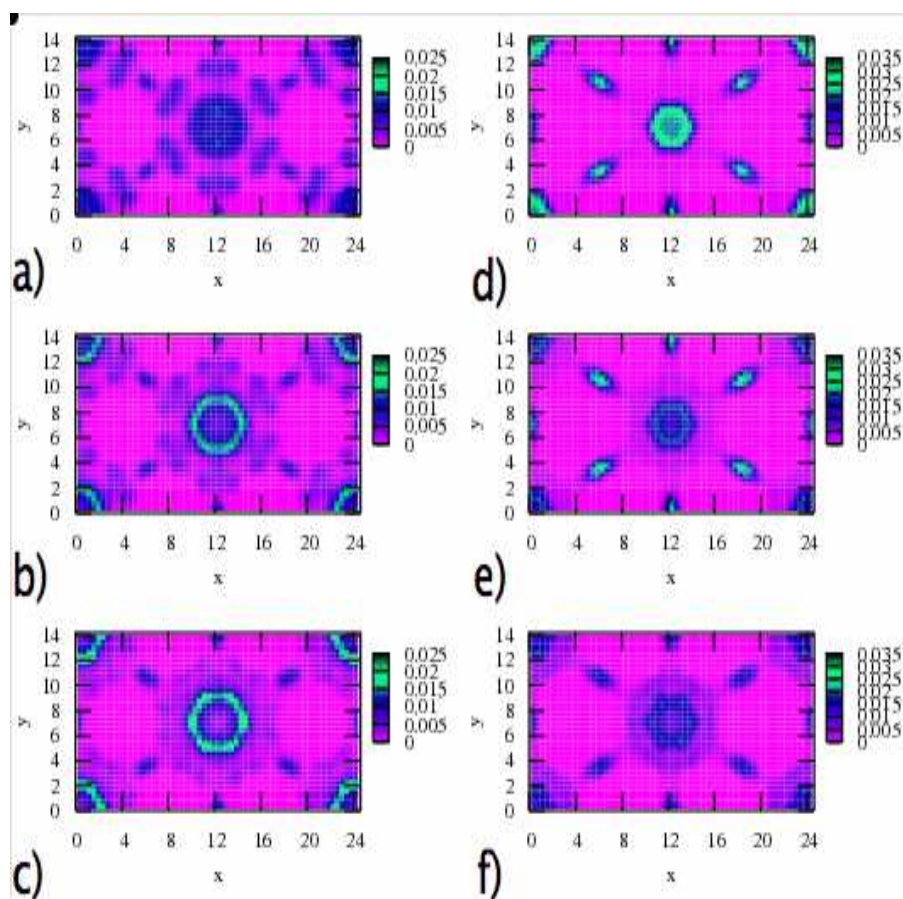


Fig. 13

1
2
3
4
5
6
7
8
9
10
11
12
13
14
15
16
17
18
19
20
21
22
23
24
25
26
27
28
29
30
31
32
33
34
35
36
37
38
39
40
41
42
43
44
45
46
47
48
49
50
51
52
53
54
55
56
57
58
59
60

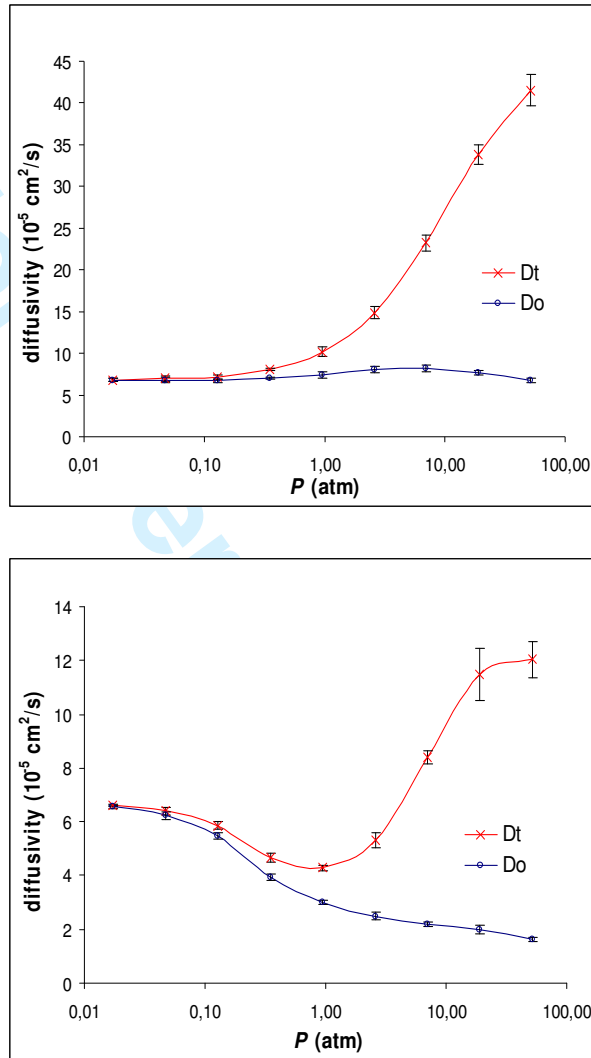


Fig. 14

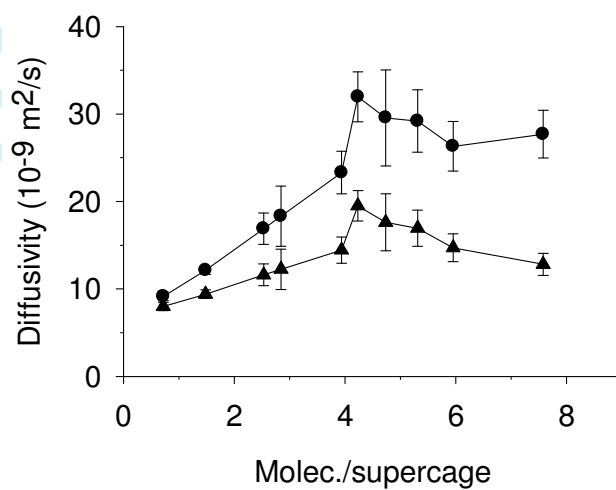


Fig. 15

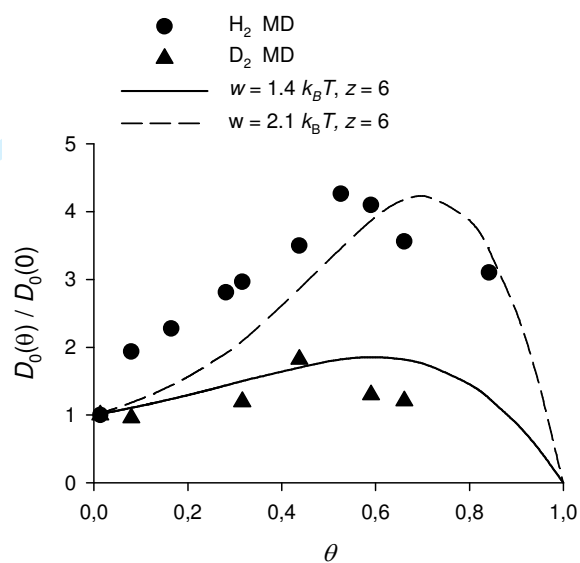


Fig. 16

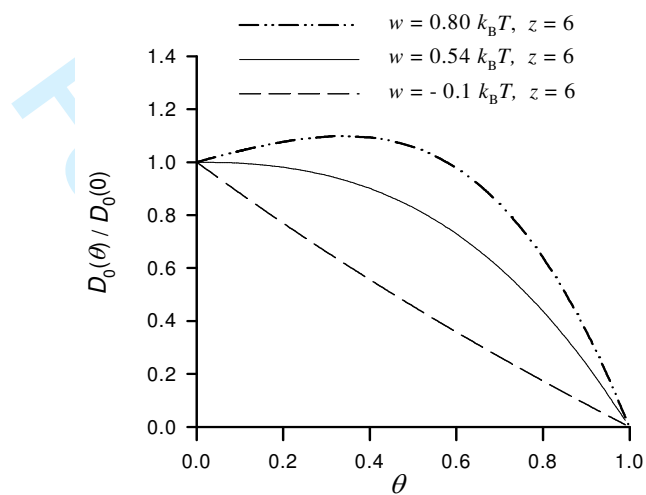


Fig. 17